International Journal of Materials and Chemistry 2012, 2(4): 178-184
DOI: 10.5923/j.ijmc.20120204.11

Effects of Heat Treatment on the Electrochemical Corrosion Behaviour of Aluminum Alloy AA8011 in 0.1M H_2SO_4 Aqueous Acid Media

Okeoma Kelechukwu B.[1,*], Owate Israel O.[2], Oguzie Emeka E.[3], Mejeha Ihebrodike M.[1]

[1]Materials Science Group, Department of Physics, Federal University of Technology, Owerri, Nigeria
[2]Materials Science Group, Department of Physics, University of Port Harcourt, Nigeria
[3]Electrochemistry and Materials Science Research Unit, Department of Chemistry, Federal University of Technology, Owerri, Nigeria

Abstract The effects of heat treatment and quenching regimens on the electrochemical corrosion behaviour of aluminium alloy AA8011 in 0.1M H_2SO_4 was studied by open circuit potential (OCP), potentiodynamic polarization (PP) and electrochemical impedance spectroscopy (EIS) measurements. Three different specimens (unheated, air quenched and oven quenched) were investigated. Polarization results show that all the specimens underwent active dissolution, with no distinct transition to passivation. Heat treatment caused the corrosion potential to shift; the oven quenched shifted to the more cathodic region, while the air quenched shifted to the anodic values. There was decrement in the rate of both cathodic and anodic partial reactions of the corrosion processes in the heat treated samples. The impedance spectra for all the specimens comprised of a high frequency capacitive loop and an inductive loop at low frequency and depict higher values of the charge transfer resistance for the heat treated specimens. All the results indicate that heat treatment increased the corrosion resistance of AA8011 in 0.1M H_2SO_4 with modifying the corrosion mechanism. The corrosion resistance obtained from the impedance measurements increased in the order unheated< air quenched < oven quenched. This trend has been correlated with the phase constituents of the different specimens as determined from the X- ray diffraction (XRD), and scanning electron microscopy (SEM).

Keywords AA8011, Heat treatment, Corrosion, Polarization, Impedance Spectroscopy, XRD, SEM

1. Introduction

Low density, good thermal conductivity, satisfactory mechanical and relatively good corrosion resistance are among the properties exploited in the usage of aluminium and its alloys in widespread industrial and domestic applications[1-3]. Particularly, aluminium alloy AA8011 is widely used in thin foil production, containers, food packaging, household foils[4, 5]. In extruded form, the alloy system is used in building, frames, automotives and aerospace industry[6]. Due to rise in demand and applications, research into the usage and the properties of this alloy when exposed to various environments has become of interest. This leads to the harnessing of special qualities of AA8011 offered as result of the elements which this alloy is composed of, coupled with the special characteristics exhibited on heat treatment and during production. For example, silicon which is present in this alloy in quantity nearly as large as iron limits the super-saturation of the matrix phase with Fe by causing a substantial level of Fe precipitation Deligic et al.[5] and Ney and Luiggi[7] studied the role of Si and Fe content on strain hardening and concluded that Fe controls the precipitation kinetics of the material. The micro-structural changes during annealing as studied by Oscarson et al.[8] showed a transition from discontinuous to continuous recrystallization as deformation increased. While Anderson et al.[9] looked at the influence of microstructure and texture on the earing behavior of Al-Fe-Si alloy system. The microstructural control in aluminium core alloy for brazing sheet application showed that an Al-Mn alloy X800 developed significantly increase in the corrosion resistance of radiator tube when exposed to service environment[10]. This behavior can be attributed to the precipitations and crystallization effects as observed by Home[11]. Wang and Jiao[4] equally observed microsegregation of a variant Al-Fe-Mn-Si system and noted the need to reduce Mn in solid solution so as to obtained desirable size of fine dispersiods. This reduction follows the transformation of the intermetallic particle[12]:

$$Al_6(Mn,Fe) \rightarrow \alpha\text{-}Al(Mn,Fe)Si \quad (1)$$

* Corresponding author:
bierechi@yahoo.com (Okeoma Kelechukwu B.)
Published online at http://journal.sapub.org/ijmc

During heating processes, the redistribution of the constituent particles which influence texture development, grain size and mechanical properties invariably affect the electrochemical properties of the material. These researchers[4, 10-11] pointed out that the presence of Fe and Si addition promotes the precipitation of the dispersoids and decreases the solubility of Mn in solid solution. The precipitation and deposition of Mn and other intermetallic particles definitely cause changes in the morphology and electrochemical stability of the alloy system. The enrichment of Mn in the second phase forms a galvanic cell effect relative to the adjacent Al alloy substrate[9]. Precipitation causes solute depletion of the matrix[13] observed. Wang and Jiao[4] noted that Mn is a beneficial element and its role in Al-Mn alloy is interpreted as reducing the difference in electrochemical potential between the matrix and the intermetallic particles. The electrochemical properties are strongly influenced by different intermetallic particles; their sizes and frequency of precipitation determine the overall corrosion behaviour[14].

The present research paper further explores the effects of heat treatment on the morphology and electrochemical characteristics of AA8011 exposed to sulphuric acid environment. The morphological study involves X-ray Diffraction (XRD) and Scan Electron Microscopy (SEM) investigations, while the electrochemical investigation deals with monitoring of the stability potential (OCP), potentiodynamic polarization (PP) and Electrochemical Impedance Spectroscopy (EIS) changes on the control/ unheated, air and oven quenched samples of the AA8011 in 0.1 M H_2SO_4 acid environment.

2. Experimental

2.1. Materials Preparation

Aluminium alloy AA8011 used in this study was obtained from First Aluminum PLC Port Harcourt, Nigeria and had the following weight-percentage composition (Si- 0.24; Fe -0.98; Cu - 0.035; Mn - 0.10; Mg = 0.009; Zn- 0.044; Ti -0.019; Al- 98.52; others the balance) The heat treated specimens were subjected to a temperature of 150℃ in a furnace for 1 h, and subsequently divided into two sets; one set was removed from the furnace and allowed to cool in open air, while the other set was left in the furnace to cool at a rate of 0.2℃/h in order to mimic the gradual cooling sequence found in heat exchanger chambers.

The untreated, air-quenched and oven-quenched samples were all machined into coupons of dimensions 1.5 cm x 1.5 cm, which were wet-polished with silicon carbide abrasive paper (from grade #200 to #1000), degreased in acetone, rinsed with distilled water and dried in warm air. These were subsequently sealed with epoxy resin in such a way that only one square surface of area 1.0 cm^2 was left uncovered.

2.2. Materials Characterization

Structural characteristics of the as received AA8011 and heat treated and quenched specimens were analysed by X-ray diffraction (XRD, XPERT-PRO) using Cu Kα radiation as well as by scanning electron microscopy (SEM, Shimadzu SSX-550). XRD measurements were undertaken to enable verification of the phase constitution before and after heat treatment/quenching. SEM imaging was used to identify surface defects (including inhomogeneities and porous intensity) arising from the different heat treatment/quenching regimen.

2.3. Electrochemical Measurements

Electrochemical experiments were conducted in a conventional three-electrode cell using a VERSASTAT 400 Complete DC Voltammetry and Corrosion System, with V3 Studio software. A platinum foil was used as counter electrode and a saturated calomel electrode (SCE) as reference electrode. The later was connected via a Luggin's capillary. The test electrolyte was 0.1 M H_2SO_4, prepared from analytical reagent grade concentrated acid using distilled water. Measurements were performed in an aerated and unstirred solutions at the end of 1 h of immersion at 30℃. Impedance measurements were made at corrosion potentials (E_{corr}) over a frequency range of 100 kHz – 10 mHz, with a signal amplitude perturbation of 5 mV. Potentiodynamic polarization studies were carried out in the potential range -0.85 to -0.45V versus the corrosion potential at a scan rate of 1mVs^{-1}. Each test was run in triplicate to verify the reproducibility of the systems.

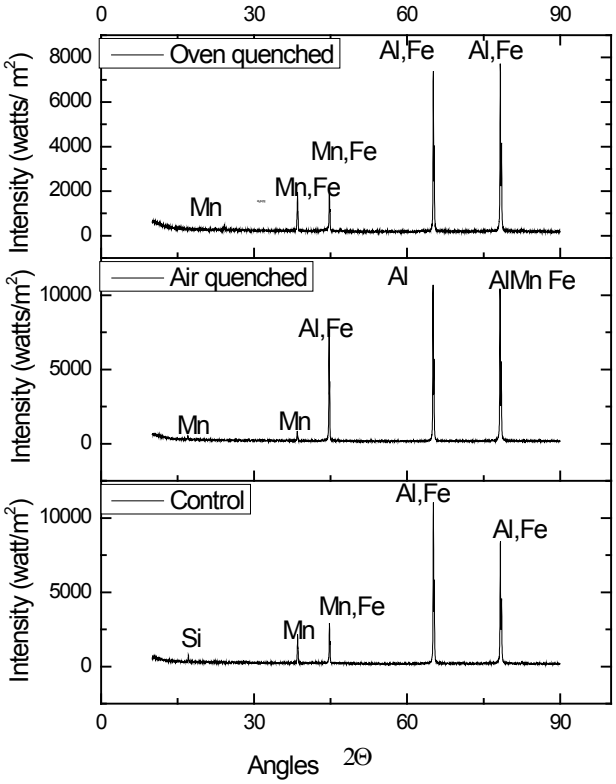

Figure 1. The XRD spectra of unheated, air quenched and oven quenched samples of AA8011

3. Results and Discussion

3.1. Structural Analysis

3.1.1. XRD spectra

Fig.1 shows the XRD patterns of the control, air quenched and oven quenched specimens of AA8011. It is easily seen that all the samples display distinct, sharp and narrow peaks signifying high crystalline nature of AA8011 alloy. The crystallite size was determined using Debye- Scherrer's formula:[15]

$$D = \frac{0.9\lambda}{\beta cos\theta} \quad (2)$$

D is the crystallite size, λ is the incident radiation wavelength which is the full width at half maximum of the profile and θ is the angular position.

From the figure it can be observed that the control and air quenched samples have higher intense peaks when compare with the oven quenched sample. This means that oven quenching lowered the degree of crystallinity of the alloy[16]. Also the number of the peaks greater than 10% of the background is the same in all the alloy samples. It means that although heat treatment did not bring about change in the number of peaks, but rather changed the type, size and frequency of the occurrence of the intermetallic particles. In the air quenched sample, for example, Al and Al_6(Fe,Mn) are observed but they are absent in other samples. There is fewer number of the detrimental crystallite Al_3Fe in the air quenched sample than in the other samples. In both control and oven quenched samples Al_3Fe are equal, but oven quenching enhanced splitting of MnFe intermetallic particle and this is absent in air quenched sample. From this observation, it is possible to imply that splitting of MnFe intermetallic particles in oven quenched specimen and formatiom of Al_6(Fe,Mn) intermetallic particles in air quenched specimen depend on the mode of heat treatment. The heat treatment caused decrease in the size of Mn, which may have been used in formation of more MnFe and Al_6(Fe,Mn) that are observed in the heat treated specimens. Further, Yanjun and Arnberg[17] observed that precipitation of Mn particles from supersaturated matrix influenced the size and composition of primary particles. The result of this investigation is in agreement with[17]. The differences observed in the different heat treatments highlight the essence of the methods in the structural characteristics of the alloy understudy. It is pertinent to point out that the high impedance observed in the oven quenched specimen may have been contributions of the effects of MnFe intermetallic particle, which are more in the oven quenched sample.

3.1.2. SEM Morphological Images

SEM micrographs of unheated, air quenched, and oven quenched specimens are illustrated in Fig 2. The unheated specimen (Fig2a) has many large, white strands, with some clustered dark spots. Fig 2b shows the oven quenched specimen, in which scanty white spots are found. In Fig.2c is the micrograph specimen for air quenched sample. It hardly contains any white spots, but some large circular dark patches are evident. From these specimens, it is clear that heat treatment dissolved the large white spots which are found in the unheated sample.

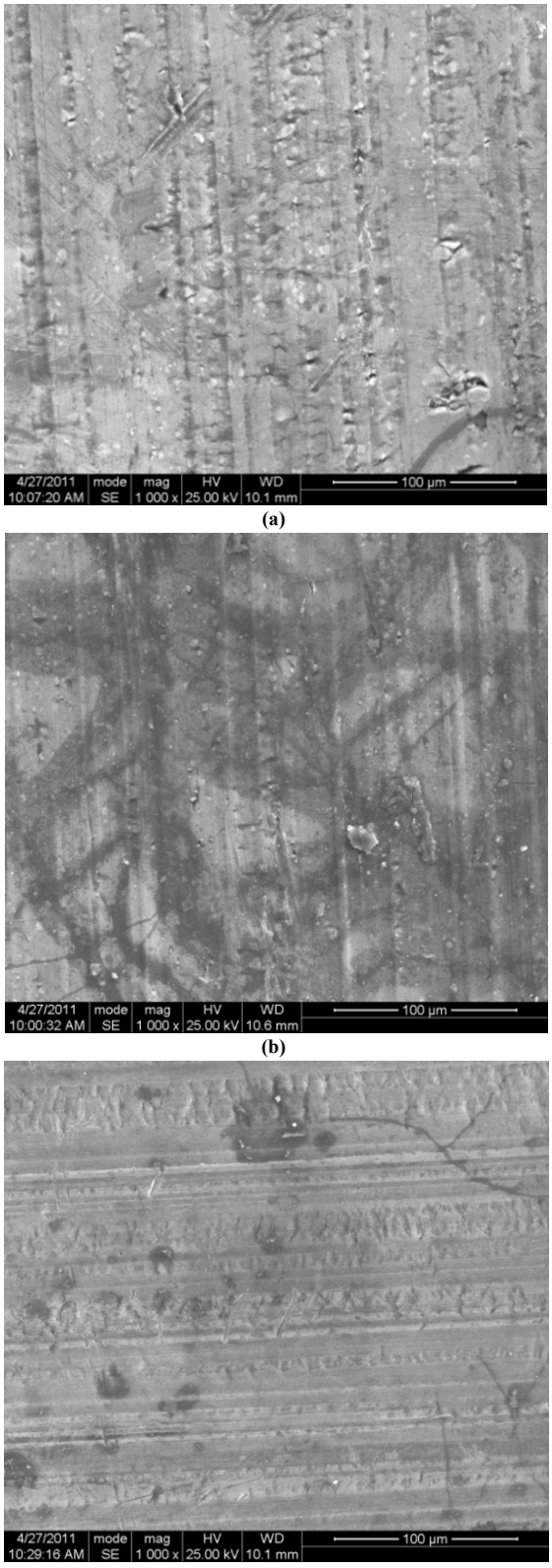

Figure 2. XRD spectra of unheated (a), Oven quenched (b) and air quenched (c) samples of AA8011

Comparison of the heated sample shows that the oven quenched specimen has tiny white spots which are absent in the air quenched sample. From these, one may deduce that heat treatment affected the morphology of AA8011 and the procedure of heat treatment goes to bring distinguishing features. This observation is in line with what was noticed in the XRD spectra in which the air quenched and oven quenched specimens have a different intermetallic constituent peaks.

3.2. Electrochemical Spectroscopy

3.2.1. Open Circuit Potential Measurements

The evolution of the open circuit potential (E_{ocp}) with time for AA8011 specimens in 0.1M H_2SO_4 solution is shown in Fig.3. A steady decrease in E_{ocp} is observed for the control specimen due to the dissolution of air formed oxide film on the electrode surface. Both heat treated samples had their E_{ocp} shifted into more positive potentials. This could be attributed to the dissolution of the precipitated intermetallic particles on the alloy surface after heating. The E_{ocp} on the air quenched specimen remained almost constant in the first 2750s before slightly decreased at the end of 1 hour. But for oven quenched specimen, the E_{ocp} decreased almost linearly within the time intervals of 250 and 2750s. It can be concluded that the heat treatment caused the oxide film to decrease the insulating properties, since high insulating films is associated with more cathodic potential as seen in the control sample.[18].

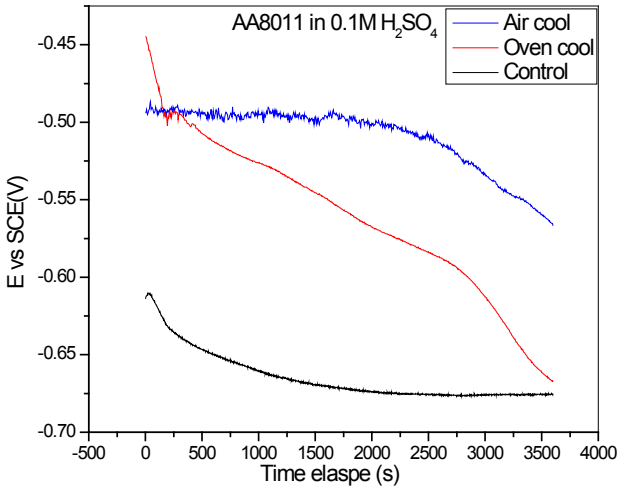

Figure 3. Open circuit potential versus time for control, oven quenched and air quenched sample of AA8011 in 0.1 M H_2SO_4 acid medium

3.2.2. Potentidynamic Polarization Measurements

The potentiodynamic polarization curves for control, oven quenched and air quenched specimens of AA8011 in 0.1 M H_2SO_4 are presented in Fig.4 and the corresponding electrochemical parameters given in Table 1. All the three samples exhibit active dissolution with no distinctive transition to passivation up to -0.45V versus SCE. The similarity of the polarization curves for the three specimens suggest comparable corrosion mechanism. It is obvious that heat treatment has a positive influence on the polarization behaviour of AA8011 in 0.1M H_2SO_4 acid environment. It decreased both anodic and cathodic current densities and shifted E_{corr} of the oven quenched specimen into more negative potentials. While the E_{corr} of the air quenched sample shifted to higher potential. The cathodic arm of the oven quenched and anodic arm of the air quenched specimen shifted to the lower current densities when compare with the control. This translated to increase in polarization resistance and hence decrease in the corrosion current densities. The positive effects of heat treatment may be attributed to the formation of less harmful intermetallic crystallites $Al_6(Fe,Mn)$ for air quenched and FeMn for oven quenched samples, whose size and frequency increased as obtained from the XRD data.[19]

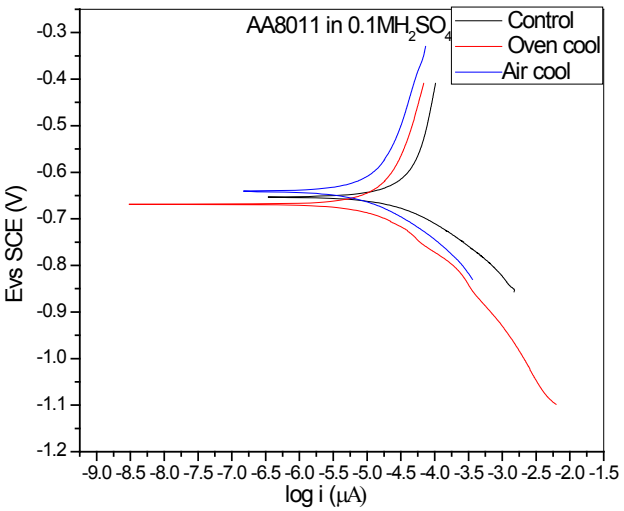

Figure 4. Potentiodynamic polarization curves for control, oven quenched and air quenched samples AA8011 in 0.1M H_2SO_4 acid medium

Table 1 that presents the polarization resistance R_p and corrosion density I_{corr} of the control, oven and air quenched specimens of AA8011 exposed to 0.1 M H_2SO_4. These are determined from Tafel segments of the respective potentidynamic curves and indicate that polarization resistance of the heat treated specimens is higher than the control sample. The air quenched sample being higher than the oven quenched sample. Conversely the corrosion current density decrease in the heat treated sample. These translate to the fact that heat treatment improved the resistance capability of AA8011 in the 0.1 M H_2SO_4 environment. The decrease in corrosion current density of oven quenched specimen relative to the control is about 0.54, while for air quenched specimen is about 0.45.

Table 1. Potentiodynamic data, Polarization resistance (R_p), and corrosion current (I_{corr}) for control, oven quenched and air quenched specimens

Specimen	$R_p(\Omega cm^{-2})$	I_{corr} (μAcm^{-2})
Control	2136.40	68.91
Oven quenched	4939.80	38.79
Air quenched	6208.86	30.95

3.2.3. Impedance Measurements

Electrochemical impedance spectra were measured at the open circuit potential for the different AA8011specimens in 0.1M H_2SO_4 solution. The obtained impedance responses are presented in Nyquist of Fig.5. All the specimens display similar impendence features; each Nyquist plot is characterized by a single depressed capacitive semicircles from high to intermediate frequencies followed by a low frequency inductive arc. The capacitive loop can be attributed to charge transfer processes associated with the effects of the double layer capacitance and its diameter is related to the charge transfer resistance (R_{ct}) at the metal/solution interface, while the inductive loop probably results from the intermediate products.

The Nyquist plots clearly indicate that heat treatment caused increase in the diameter of the capacitive arc, hence the R_{ct} which corresponds to an increase in the corrosion resistance of AA8011 in 0.1 M H_2SO_4 solution. This effect is more pronounced for oven quenched sample and points toward the low corrosion susceptibilities of the heat treated samples in the sulphuric acid medium. R_{ct} increase in the order unheated< air quenched < oven quenched. This does not agree with the trend of corrosion resistance predicted by the polarization data, possibly because of effects of different heat treatment on the Tafel constant.

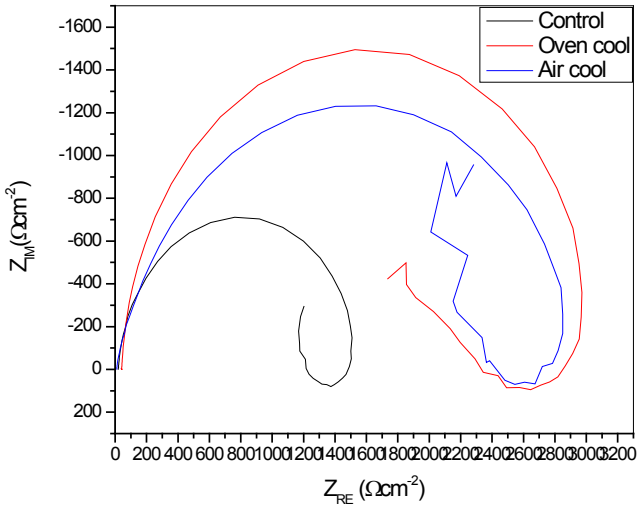

Figure 5. Electrochemical impedance spectra of unheated/ control, oven quenched and air quenched specimens of AA8011 in 0.1M H_2SO_4

The corrosion behavior of the heat treated specimens can be related to the features of the intermetallic particles arising from the heat treatment as illustrated in the XRD spectra (Fig.1). The corrosion behavior of the heat treated samples can be better explained by the fact that the comparatively large and less harmful particles result from the heat treatment and quenching processes. These provide low population of corrosion sites as well as low volume grain boundaries which reduce corrodent attack and corrodent transport to the alloy surface.

To obtain the numerical values of the various impedance parameter presented in table 2, the impedance spectra were analyzed by fitting into Fig.6, equivalent circuit $R_s(QR_1(R_2L))$. R_s is the solution resistance which is the uncompensated resistance between the working electrode and the reference electrode; R_1 is the leakage resistance that represents the charge transfer resistance associated with the constant phase element (CPE) Q, which is used to model deviation from an ideal capacitor. These are in parallel with R_2 which is the resistance offered to the migrating ions in the solution that manifested in the magnetic fields with its associated series inductance L, which become dominant within a certain frequency range for a particular specimen.

Table 2. Data obtained from the impedance spectra

Parameters	Control	Oven quenched	Air quenched
R_s(Ωcm^{-2})	20.04	41.24	9.714
Qx10^{-5}	1.72	0.98	1.46
n	0.9399	0.9627	0.8663
R_1 (Ωcm^{-2})	1539	3010	2971
L(mH)	4395	7148	8044
R_2(Ωcm^{-2})	6315	8794	14950
Values at maximum imaginary loop			
F_{max} (Hz)	7.943	6.310	6.310
Z_{im}(Ωcm^{-2})	711.54	1495.19	1230.40
Z_{re} (Ωcm^{-2})	760.46	1527.19	1402.69
C_{max} x10^{-5} (Fcm^{-2})	2.816	1.687	2.050
Values at maximum real loop			
F_{max}(Hz)	0.158	0.158	0.126
Z_{im}(Ωcm^{-2})	80.48	94.81	69.56
Z_{re}(Ωcm^{-2})	1216.72	2438.64	2481.46
L_{max}(mHcm^{-2})	80.81	95.22	55,03
Double layer capacitance			
C_{dl} (μF)	13.642	8.573	8.999

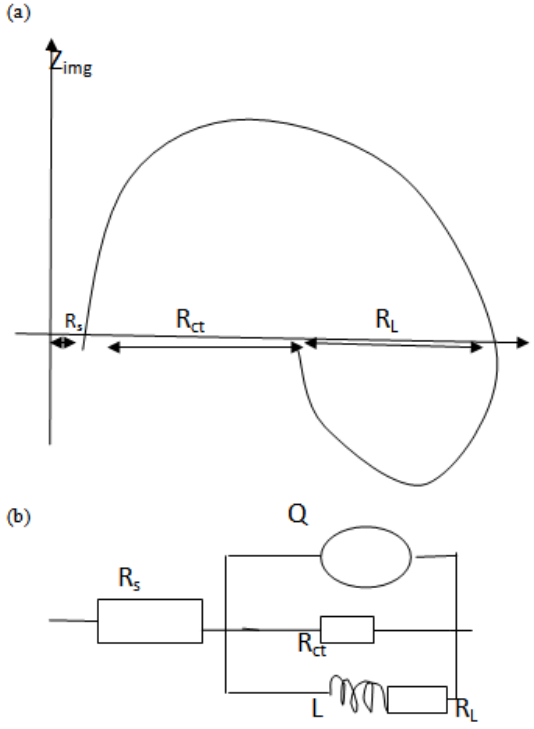

Figure 6. The complex impedance diagram (a) and the equivalent circuit diagram for total impedance (b) for the theoretical calculations

From Fig 6, the total impedance of the circuit can be calculated using eq. (4-7)

$$Z_L^{-1} = \frac{R_{L-j\omega L}}{R^2-(\omega L)^2} \quad (4)$$

$$Z_{cpe}^{-1} = Q^{-1}(i\omega)^{-n} \quad (5)$$

$$Z_{Tol}^{-1} = R_{ct}^{-1} + Z_{CPE}^{-1} + Z_L^{-1} \quad (6)$$

$$Z_{Tol}=R_s+\{\frac{R_L^2-(\omega L)^2+Q(i\omega)^n R_{ct}(R_L^2-(\omega L)^2]+R_{ct}(R_L-j\omega L)}{R_{ct}[R_L^2-(\omega L)^2]}\}^{-1} \quad (7)$$

Where Z_{CPE} is the impedance due to the constant phase element, and Z_L is the resultant impedance due to series combination of inductance L and resistance, R_L. is the complex impedance plot of Fig. 6b, the value of R_{ct} represents the intersection point of the low frequency semicircle on the real axis , for $\omega \rightarrow 0$. In general, the value of this intersection may be used to obtain the apparent ac polarization resistance R_p[20]

$$R_{p=\lim_{\omega\to 0}|Z_{re}|}$$

From the results presented in table 2, the effects of heat treatment are very pronounced, the values of CPE Q decreased, and oven quenched being the least. The non-ideality in capacitive behavior n changed in the heat treated specimen, with air quenched deviating most. Other parameters R_{ct}, R_L, and L, all increased in the heat treated samples, with the air quenched sample being higher in each case. These high resistance values give credence to the low current densities observed in the potentiodynamic polarization. The capacitance at maximum imaginary impedance determined by

$$C = \frac{1}{Zimp\omega} \quad (8)$$

decreased in the heat treated specimens, oven quenched samples being the least. Where Z_{imp} is the maximum imaginary impedance and ω is the angular frequency at the maximum impedance. From the above information, it implies that the thickness of oxide film increased for the heat treated sample. This indicates that the heat treatment may have caused the growth of oxide layers and corrosion products that aided the blockage of active sites which translated in the high impedance in the heat treated samples of AA8011 within 0.1 M H_2SO_4. To support this result, double layer capacitance C_{dl} which is used as index of corrosion rate since it is proportional to it is calculated using the equation (9) below

$$C_{dl} = [QR^{1-n}]^{1/n} \quad (9)$$

Where Q is the constant phase element, R is the resistance associated with it, and n is the frequency that measures the degree of inhomogeneity. The calculated value of double layer capacitance for control, oven quenched and air quenched specimens show that the heat treatment caused the double layer capacitance to decrease. The value for oven quenched specimen is smaller than for air quenched specimen. These low values of the double layer capacitance are evidences that the heat treatment caused the alloy to develop insulating oxide layers which is larger for oven quenched specimen[16, 20-22] and decrease in oxide film dielectric constant.[23] These are supported by the XRD and SEM data presented. This positive effect of AA8011 in 0.1 M H_2SO_4 opens up a window for further research and applications of this alloy.

4. Conclusions

The electrochemical behavior of unheated and heated specimens of aluminium alloy AA8011 in 0.1M H_2SO_4 acid environment were investigated after the XRD and SEM measurements of the samples were taken.

- The XRD profiles showed, sharp, narrow, high peak values for all the alloy samples, showing high crystallinity of the AA8011 alloy sample.
- The heat treatment did not caused cause increase splitting of the crystallites but caused the formation of less harmful crystallite Al_6(FeMn) for air quenched sample and increase in the crystallite FeMn in the oven quenched .
- The SEM data revealed a decrease in the size number and grain volume fraction of the crystallites.
- The reduction in the size and grain volume fraction observed in the heat treated specimens translated to increase in corrosion resistance.
- The OCP, PP, and EIS all buttress the effect of heat treatment on the corrosion resistance of the AA8011 in the acid environment; this is shown in lower current densities, higher capacitive loops and larger values of simulated parameters.
- The lower values of double layer capacitance and higher thickness of the oxide layer might have contributed immensely to the blockage of active sites.
- The information garnered from this research forms and opens a window of application of this alloy in service environment.

REFERENCES

[1] Tierce, S, Pebere, N, Blanc, C, Casenave, C, Mankoiski, G, Robidou, H (2006) Corrosion behaviour of brazing material AA4343. Electorchim Acta, vol 53, 3, 12 p 1092.

[2] Wang, S.S, Cheng, M.D, Tsao, L.C, Chuang, T.H, (2001) Corrosion behaviours of Al-Si-Cu (Sn, Zn) brazing filler metals mat chara 47, 4014

[3] Wang, G and Jiao, H, (2010), Microstructural Effects in Corrosion of Aluminium tube alloys, Trans. Nonferrous Met. Soc. China 21, 1193-1198.

[4] Goncalves, W.F.O, Zoqui, E.J, Paes, M,(2006) Effect of Grain refining and Homogenizing treatment on Al-Fe-Mn-Si cast alloys, 17th CBECIMat- Congresso Brasileiro de Engenharia e Clencia dos materials, 5080-5088.

[5] Delijic, K, Asanovic, V, Radonjic, D, Mechanical and corrosion properties of Aa8011 sheets and foils, Mat. Tech. 40(3) 83-88.

[6] Borodiak, M, Pinheiro, F.P, and Pacs, Marcedo, (2012) Metallurgical characterization of Aluminium alloy by matrix dissolution, Light metal 2012,Ed. Carlou E.S, TMS.

[7] Ney, J and Luiggi, A (1998) Charaterization by thermoelectric power of commercial aluminium- Iron- silicon alloy AA8011 during isothermal precipitation, Metall. Mater. Trans. 19A, 2669.

[8] Oscarson , A, Lehtinen, B, Hutchinson, B, Ekstron, H. E, Bate, P, Haggstron, L, Ghandour, A.M (1994) in preceeding of the 4th International Conference on Aluminum alloys. Altlanta. Georgia, USA Vol. III, 144.

[9] Anderson , B, Naess, S.E. (1987) in Proceedings of the 8th International Light Metals Congress, Leoben. Viena, (Aluminium Verglag GmbH), 526

[10] Marshall, G.J, Bolingbroke, R.K, Gray, A (1993) Microstructural control in aluminium core alloy for brazing sheet applications, Metallurg. Mat. Trans. A 1935-1942.

[11] Howe, J.M.(1986) Metallographical and differential scanning calorimetry analyses of precipitation and crystallization in an Al-Mn alloy, Metall. Trans. A. Vol. 17, Iss. 4, pp593-605.

[12] Bahadur, A (1988), Intermetallic phases in Al-Mn alloys, Journ. of Mater. Sci. 23, 48-54.

[13] Li, Y.J, Arnberg, L, (2003) Evolution of eutectic intermetallic particles in DC-cast AA3003 alloy during heating and homogenization, Mater. Sci. and Eng. A, 347.

[14] Slamova, M, Ocenasek, V, Cieslar, M, Chalupa, B, Merle, P (2000) "Differences in structure evolution of twin roll cast AA8006 and AA8011 during annealing". Mater. Sci. Forum Vol. 331-337, 829-834.

[15] Cullity, B.D, Element of X-Ray Diffraction, 2nd ed. 1972, Addison-Wesley, Pub. Coy, California, USA.

[16] Ruhi,G, Modi, O.P, Jha, A.K, Singh, I.B, (2009) Characterization of corrosion resistance properties of sol-gel aluminium coating in marine water environment , Ind. Journ. Chem. Techn. Vol.16, 216-220

[17] Yanjun, L, Amberg, L (2003), "Precipitation of dispersoids in DC cast AA3103 alloy during heat treatment" Light metal 2003, 991-997.

[18] Szklarska- Smialowska, Z, (1999), Pitting Corrosion of aluminium, corros.Sci. 41, 1743- 1767.

[19] Birbilis, N, Buchheit, R.G, (2005) "Electrochemical Characteristics of Intermetallic Phases in Aluminium Alloys: An Experimental Survey and Discussion" Journ. Electrochem. Soc. 152 (4) B140-B151.

[20] Ambat , R, Davenport, A.J, Scamans, G.M, Afseth, A, (2005) Electrochemical behaviour of the active surface layer on rolled aluminium alloy sheet, J. Electrochem. Soc. B, 151(1),53-58.

[21] Liu, Y, Chen, Y. F, (2010), The role of second phase particles in pitting corrosion ofAL alloy in NaCl solution, mater. And corros, vol.61 iss 3, 211-217.

[22] Metikos-Hukovic, M, Babic, R, Grubac, Z,(2002) The study of aluminium corrosion in acidic solution with nontoxic inhibitors, Journ. of Appl. Electrochem. 32, 35-41.

[23] Osorio, W.R., Cremasco, A, Andrade, P.N, Carcia, A. Caram, (2010), Electrochemical behavior of centrifuged cast and heat treated Ti-Cu alloys for medical applications. Electochimica Acta 55, 759-770.